Investigation on Mechanism of Catalysis by Pt−LiCoO 2 for Hydrolysis of Sodium Borohydride Using X-ray Absorption

ARTICLE *in* THE JOURNAL OF PHYSICAL CHEMISTRY B · MAY 2008

Impact Factor: 3.3 · DOI: 10.1021/jp075592n · Source: PubMed

9 AUTHORS, INCLUDING:

Ren-Shyan Liu
Taipei Veterans General Hospital
592 PUBLICATIONS **7,337** CITATIONS

SEE PROFILE

Hao Ming Chen
National Taiwan University
61 PUBLICATIONS **1,648** CITATIONS

SEE PROFILE

Investigation on Mechanism of Catalysis by Pt−$LiCoO_2$ for Hydrolysis of Sodium Borohydride Using X-ray Absorption

R. S. Liu,*,† H. C. Lai,† N. C. Bagkar,† H. T. Kuo,† H. M. Chen,† J.-F. Lee,‡ H. J. Chung,§ S. M. Chang,§ and B. J. Weng§

Department of Chemistry, National Taiwan University, Taipei, Taiwan 106, National Synchrotron Radiation Research Center, Hsinchu, Taiwan 300, and Chung-Shan Institute of Science and Technology, Taiwan

Received: July 17, 2007; In Final Form: December 28, 2007

The synthesis of platinum nanoparticle loaded $LiCoO_2$ (Pt−$LiCoO_2$) was carried out successfully by an impregnation method followed by sintering at different temperatures. The catalytic role of Pt−$LiCoO_2$ composite in hydrogen generation during hydrolysis of sodium borohydride ($NaBH_4$) was studied for fuel cell applications. X-ray diffraction (XRD), transmission electron microscopy (TEM), and inductively coupled plasma-atomic emission spectroscopy (ICP-AES) have been used to elucidate the structural and catalytic properties of Pt−$LiCoO_2$. It was found that the 15 wt % of Pt nanoparticles on $LiCoO_2$ sintered at 450 °C support showed the maximum efficiency for the catalysis reaction of hydrogen production. X-ray absorption near edge structure (XANES) analysis and extended X-ray absorption fine structure (EXAFS) analysis using a synchrotron radiation source were performed to carry out *ex situ* measurements in order to understand the mechanism of the catalytic process for the production of hydrogen during the hydrolysis of $NaBH_4$. Co K-*edge* XANES showed a small percentage of cobalt in the metallic form after hydrogen generation which suggests the reduction of the cobalt during the hydrolysis of $NaBH_4$.

1. Introduction

The growing demand for the use of hydrogen energy has accelerated research for hydrogen generation and its storage for fuel cell applications. Hydrogen is being considered as a clean energy source mainly because of its advantages in overcoming problems with energy resources and in environmental issues.[1] One of the important advantages of hydrogen fuel economy is that energy can be stored in the form of hydrogen and can be transported anywhere as the need arises.[2] Hydrogen can be produced from either splitting of water (electrolysis) using renewable electricity or during the microbial and biological reaction from suitable hydrogen-containing sources.[3−5] Hydrogen generation from the chemical hydrolysis of a metal hydride has been extensively studied as a promising candidate.[6] One of the most used metal hydrides is sodium borohydride which has intrinsically high storage density up to 10.8 wt % for hydrogen and can be used in combination to yield practical generation systems with proper engineering.[7−11] Hydrogen can be generated in a double amount of its stored content by a controllable heat releasing reaction with no side reaction or volatile byproducts, and the generated hydrogen is very high purity which can be combined with a proton exchange membrane (PEM) in fuel cell applications.[12]

The hydrolysis of sodium borohydride generally results in the formation of sodium metaborate because of which the pH of the solution decreases and the reaction rate becomes sluggish. Also the self-hydrolysis of sodium borohydride at low pH value results in the uncontrolled release of hydrogen. However, these difficulties are overcome by increasing the pH of the solution above 9. The pH-stabilized sodium borohydride hydrolysis is then accelerated by using a suitable catalyst such as platinum or ruthenium for achieving higher efficiencies for hydrogen generation.[13] The standard enthalpy change for the catalysis reaction is 300 kJ and half of the hydrogen produced is derived from the water and sodium borohydride each. The role of heterogeneous catalyst is to produce hydrogen from an alkaline solution of sodium borohydride since in the absence of catalyst it does not produce appreciable quantities of hydrogen. The effect of hydrolysis temperature, NaOH concentration, and sodium borohydride concentration on the rate of reaction has been studied in detail which gives important understanding about the kinetics of the hydrolysis of sodium borohydride.[14−16] Recently a very effective methodology was reported for studying the kinetics of Pd-catalyzed hydrolysis of sodium borohydride wherein the different interemediates generated were investigated using nuclear magnetic resonance (NMR) technique.[17] In this case the hydrolysis followed first-order kinetics with respect to concentration of both substrate and catalyst.

The catalyst generally used for the hydrolysis of sodium borohydride include colloidal metal clusters of noble metals, active carbon, metal halides, and metal nanoparticles supported on ion-exchange resin beads.[7,9] The platinum nanoparticles impregnated on carbon support has been extensively studied for its chemical structure on carbon support by *ex situ* X-ray photoelectron spectroscopic (XPS) measurements.[18] The use of X-ray absorption (both X-ray absorption near edge structure (XANES) analysis and extended X-ray absorption fine structure (EXAFS) analysis using synchrotron radiation can provide a wealth of information regarding the local structure and electronic state of the dispersed metal particles that form the active sites in fuel cell catalysts.[19] The position of the absorption edge is related to the oxidation state of the absorbing atom, and the

* To whom correspondence should be addressed. E-mail: rsliu@ntu.edu.tw. Phone: +886-2-33661169. Fax: +886-2-3629-3121.
† National Taiwan University.
‡ National Synchrotron Radiation Research Center.
§ Chung-Shan Institute of Science and Technology.

10.1021/jp075592n CCC: $40.75
Published on Web 04/03/2008

detailed features can provide the identification of the neighbors, coordination geometry, and, in the case of clusters of atoms, particle size and morphology. EXAFS analysis, in particular, gives valuable information about the changes in the local structural environment, coordination number, and bond length of the absorbing atom. EXAFS measurements of H_2PtCl_6 impregnated on activated carbon suggested the detailed chemical information about the platinum chemical structure on the support which showed the absence of Pt−Pt peaks in the catalyst.[20] The more detailed study of *in situ* as well as *ex situ* XAS measurements on the H_2PtCl_6 impregnation onto activated carbon followed by electrochemical reduction showed the reduction of platinum compound to Pt(II), and hydrogen generation was found to be independent of the platinum species reduction.[21] The platinum nanoparticles loaded on the other supports such as metal oxides also showed remarkably higher efficiencies for hydrogen production using sodium borohydride.[22] However, there are very few reports on the structural changes occurring at the active catalyst impregnated on metal oxide such as $LiCoO_2$ surfaces during the heterogeneous catalysis of hydrolysis of sodium borohydride. Hence, we have used XAS measurements using both XANES and EXAFS for probing the structural and local environmental changes occurring in the vicinity of both active Pt catalyst as well as $LiCoO_2$ support during the hydrolysis. Such studies will be beneficial in deducing the effective catalyst concentration and its environment for the efficient generation of catalyst.

2. Experimental Section

2.1. Materials. All chemicals, H_2PtCl_6 (99.5%) from Alfa, $LiCoO_2$ (99.8%) from Aldrich, sodium borohydride (99.0%) from Aldrich, nafion (5%) from Dupont, and Pt/C (5%) from Acros, were used without further purification. All the solutions were prepared using deionized water produced using a Milli-Q SP ultrapure-water system from Nihon Millipore Ltd., Tokyo.

2.2. Synthesis of Pt−$LiCoO_2$ Composite Catalyst. The platinum nanoparticle loaded $LiCoO_2$ composite catalyst samples were synthesized using conventional impregnation method. In a typical experiment H_2PtCl_6 and $LiCoO_2$ were mixed in a desired ratio such that concentration of Pt varies as 5, 10, 15, 20, and 30%. The composite samples were then heated after sonication for 20 min in the furnace at 250 °C for 5 h in air atmosphere. The samples were then cooled to room temperature and thoroughly mixed by grinding. The catalyst samples were then sintered in air atmosphere at 450 °C for 5 h.

2.3. Hydrogen Generation Experiments. The catalytic process was monitored by measuring hydrogen generation rates for the hydrolysis of $NaBH_4$ using different concentrations of platinum nanoparticle loaded $LiCoO_2$ support. In a typical experiment, 0.1 g of sodium borohydride and 10 mg of Pt−$LiCoO_2$ were mixed in stoppered flask, and to this 25 mL of deionized water was added. The hydrogen generated during the hydrolysis of $NaBH_4$ was collected, and its volume was measured using water trap method. The change in the volume in the cylinder was recorded at the time interval of 5 min.

2.4. Sample Preparation for *ex Situ* XANES and EXAFS Analysis. The samples for *ex situ* analysis were prepared in two steps. A 0.4 g amount of the composite catalyst sample was dissolved in few drops of nafion, 0.5 mL of deionized water, and 1 mL of isopropyl alcohol and mixed together to form the slurry of the catalyst. The slurry was then mixed thoroughly in mortar to get smaller sized particles and then pasted on the carbon paper to form the thin film of catalyst on the carbon paper which was then heated in oven at 120 °C. The process is repeated several times until all the slurry containing catalyst was transferred on the carbon paper and again heated for 3 h in oven to get a powder sample.

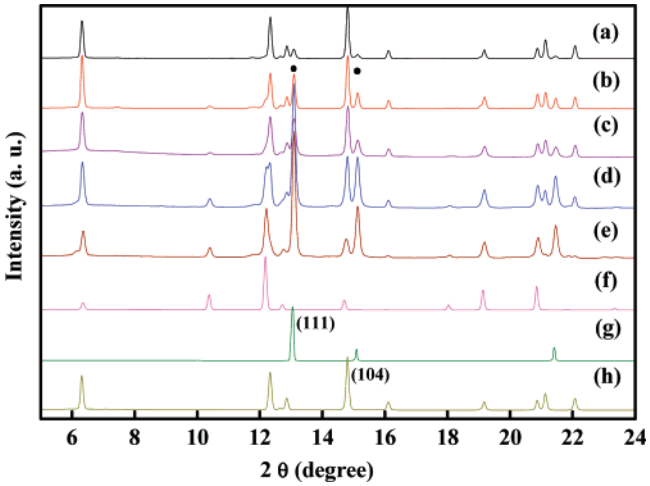

Figure 1. XRD patterns of (a) 5, (b)10, (c)15, (d) 20, and (e) 30 wt % of Pt−$LiCoO_2$, before catalysis reaction, (f) Co_3O_4, (g)$LiCoO_2$, and (h) Pt foil.

2.5. Characterization. X-ray diffraction (XRD) measurements were carried out using BL17A1, a synchrotron radiation X-ray source at the National Synchrotron Radiation Research Centre. The surface morphology was examined by transmission emission microscopy (TEM) using a JEM-2000EX microscope operated at 200 kV. The Pt L_{III}-edge and Co K-edge X-ray absorption near-edge structure (XANES) was recorded in transmission mode for synthesized powder mounted on Scotch tape, at a BL17C Wiggler beamline by using a double-crystal Si (111) monochromator. The X-ray high harmonic was detuned by mirrors. Reference spectra were simultaneously collected for each *ex situ* spectrum by using Co and Pt metal foil. Wiggler-C beamline of the National Synchrotron Radiation Research Center (NSRRC), Taiwan, has been used for such experiments.

2.6. EXAFS Data Analysis. For EXAFS data analysis, raw X-ray absorption data were analyzed following standard procedures,[23] including pre-edge and post-edge background subtraction, normalization with respect to edge height, Fourier transformation, and nonlinear least-squares curve fitting. The fits were performed using k^3 weighting and included background refinement. The normalized k^3-weighted EXAFS spectra, $k^3\chi(k)$, were Fourier-transformed in the k range from 2.5 to 14 $Å^{-1}$ to reveal the contribution of each bond pair on the Fourier transform (FT) peak. The experimental Fourier-filtered spectra were obtained by performing an inverse Fourier transformation with a Hanning window function with r between 1.9 and 3.2 Å. The Pt and Co edge data were analyzed simultaneously.

3. Results and Discussion

In order to determine the effective concentration of platinum on $LiCoO_2$ support responsible for the highest catalysis rate during the hydrolysis of sodium borohydride, different amounts of Pt loaded on $LiCoO_2$ were characterized by XRD and XAS techniques. XRD using synchrotron radiation source was used for structural determination of the composite catalyst. XRD patterns of 5, 10, 15, 20, and 30 wt % of Pt loadings on $LiCoO_2$ are shown in the Figure 1. It was observed that Pt (111) peak intensity is increased when the platinum content is increased in the catalyst composite. XRD pattern of 5 wt % Pt−$LiCoO_2$ phase is similar to the $LiCoO_2$ phase whereas for the higher concentrations of Pt−$LiCoO_2$, an impurity peak due to Co_3O_4

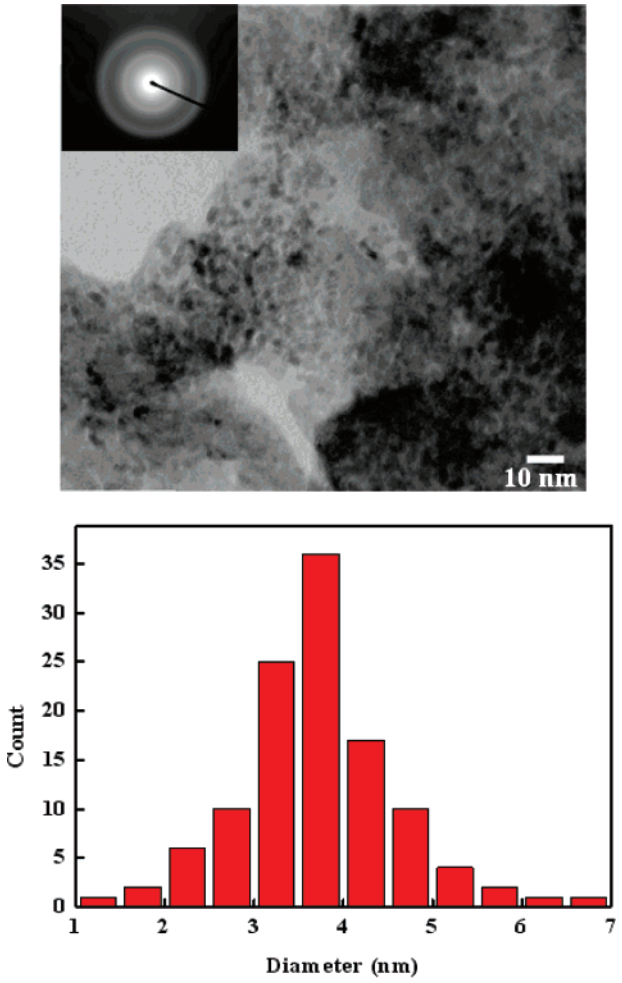

Figure 2. (a) TEM image and electron diffraction pattern, (b) particle size distribution of 15 wt % Pt−$LiCoO_2$ with average particle size of 3.7 ± 0.8 nm.

TABLE 1: Structural Parameters and Particle Sizes of 5, 10, 15, 20, and 30 wt % of Pt−$LiCoO_2$

concentration of Pt in $LiCoO_2$	H_2PtCl_6 (wt %)	Pt (wt %) (ICP-AES)	XRD peak intensity Pt(111)/$LiCoO_2$(104)
5% Pt−$LiCoO_2$	5	3.8	0.17
10% Pt−$LiCoO_2$	10	7.2	0.65
15% Pt−$LiCoO_2$	15	12	0.74
20% Pt−$LiCoO_2$	20	18	2.45
30% Pt−$LiCoO_2$	30	28	7.3

was observed. Co_3O_4 impurity originated from the decomposition of $LiCoO_2$ at higher sintering temperatures.[24] The platinum content determined by ICP-AES for 5, 10, 15, 20, and 30 wt % of Pt on $LiCoO_2$ is shown in Table 1. With the increasing concentration of H_2PtCl_6 precursor used in the synthesis, it was found that the Pt content (including Pt loaded on $LiCoO_2$ and segregated as Pt clusters) in $LiCoO_2$ is also increased.

TEM image and electron diffraction pattern of 15 wt % of Pt−$LiCoO_2$ is shown in Figure 2(a). The platinum nanoparticles are identified as small dark dots on the gray $LiCoO_2$ support, and average particle size was derived after analyzing nearly 150 particles by TEM. A uniform particle size distribution with an average particle size of 3.7 ± 0.8 nm was observed for 15 wt % of Pt−$LiCoO_2$, which suggests that the platinum nanoparticles are well dispersed in $LiCoO_2$ support as shown in Figure 2(b). Therefore, the uniform particle size of platinum is expected to provide larger relative surface areas of platinum active sites, resulting in higher utilization of Pt in the hydrolysis reaction.

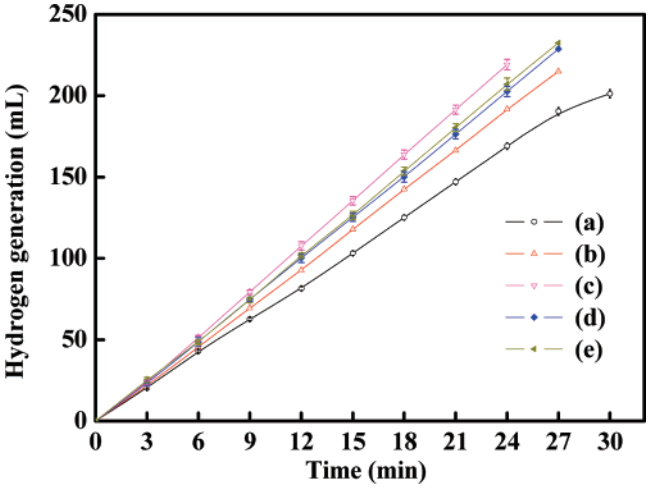

Figure 3. Hydrogen generation of (a) 5, (b) 10, (c) 15, (d) 20, and (e) 30 wt % of Pt−$LiCoO_2$.

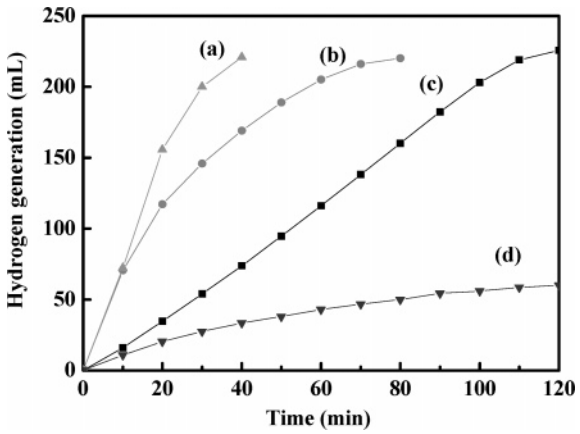

Figure 4. Hydrogen generation comparison of (a) 5 wt % Pt−$LiCoO_2$, (b) Pt black, (c) $LiCoO_2$, and (d) blank.

Figure 3 shows the volume of hydrogen generated for different concentrations of Pt−$LiCoO_2$. It was observed that 15 wt % Pt−$LiCoO_2$ showed the maximum hydrogen generation rate suggesting the optimum concentration of Pt for catalysis of sodium borohydride. However, the hydrogen generation rate is decreased for higher concentration which can be attributed to reduction in the surface area due to aggregation of platinum nanoparticles. Another reason for the observed reduced rate is the presence of impurity in 20 and 30 wt % Pt−$LiCoO_2$, which is responsible for affecting the catalytic activity of the composite.

In order to investigate the kinetics of catalysis reaction, hydrogen generation was monitored at different time intervals, and hydrogen generation rates of 5 wt % Pt−$LiCoO_2$ were compared with pure water without catalyst as blank, pure platinum nanoparticles (platinum black, particle size of 5 nm) and $LiCoO_2$ support. The blank measurements were performed to evaluate their involvement in the catalytic hydrolysis of sodium borohydride. Figure 4 shows the hydrogen generated for different catalysts used for the hydrolysis of sodium borohydride. It was found that Pt−$LiCoO_2$ showed the highest hydrogen generation rate followed by a decrease for pure platinum nanoparticles and pure $LiCoO_2$ and water in that order. Since pure $LiCoO_2$ also showed significant catalysis behavior, it is reasonable to believe that the catalytic activity of Pt−$LiCoO_2$ results from combined contribution of both platinum nanoparticles and pure $LiCoO_2$ in the hydrogen generation during the catalytic hydrolysis of sodium borohydride. The hydrogen production using 5 wt % Pt−$LiCoO_2$ and $LiCoO_2$

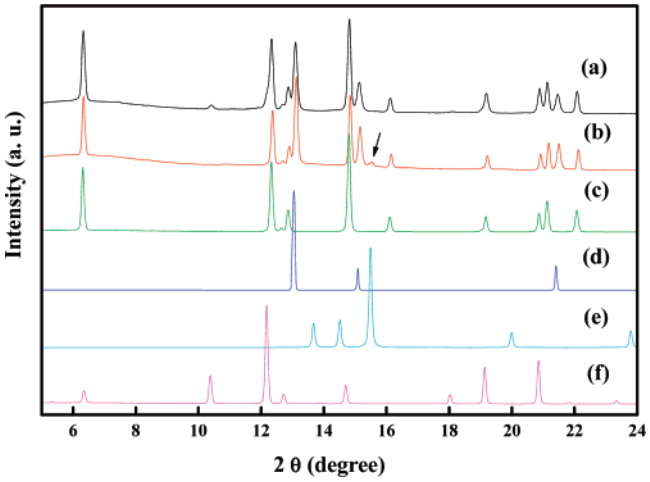

Figure 5. XRD patterns of 15 wt%Pt−$LiCoO_2$ (a) before and (b) after catalysis reaction compared with pure (c) $LiCoO_2$, (d) Pt foil, (e) Co, and (f) Co_3O_4.

follows zero-order kinetic dependence on the Pt concentration. The hydrogen generation rate is 2.0×10^{-5} g/s and 8.61×10^{-5} g/s for pure $LiCoO_2$ and 5 wt % Pt−$LiCoO_2$, respectively. It suggests that the rate is independent of sodium borohydride concentration and depends on the surface area of the catalyst.[25] The activation energy involved in the H_2 production was determined by using rate constants at different temperatures. The slope of ln(k) versus the reciprocal of absolute temperature ($1/T$) gave the activation energy of 45 kJ mol^{-1}, which is similar to the reported values.[25]

The *ex situ* analysis of Pt−$LiCoO_2$ catalyzed hydrolysis of sodium borohydride was studied by using a synchrotron radiation source to study the structural changes occurring during the catalysis reaction process in detail. We have used 15 wt % Pt−$LiCoO_2$ for analysis since it gives the maximum H_2 generation rate and better uniformity as compared to other samples. XRD measurements using synchrotron beamline BM01C2 were carried out on pure $LiCoO_2$ and 15 wt % Pt−$LiCoO_2$ to study the role of catalyst during hydrolysis. XRD patterns were recorded before and after the catalysis reaction to study the change in the structure of the catalyst. Figure 5 shows the XRD pattern of 15 wt % Pt−$LiCoO_2$ compared with pure $LiCoO_2$ and Co and Pt foil. It was observed that the structure of pure $LiCoO_2$ during the hydrolysis for different time periods remains the same whereas the XRD pattern of Pt−$LiCoO_2$ showed remarkable changes with time. The arrow in Figure 5 indicates the appearance of the peak due to Co after the hydrolysis reaction. We believe that Pt plays an important role as an active center during the hydrolysis causing the reduction of Co^{3+} ions to Co metal through the electron transfer as evident from the XRD measurements. During the hydrogen generation, the concentration of BH_4 ions in the vicinity of catalyst surface decreases and more BH_4 ions should absorb on the Pt surface which will be helpful for the electron transfer from BH_4 to $LiCoO_2$, liberating hydrogen. Since nanosized platinum particles offer a large surface to BH_4 ions, the role of Pt can be understood as a mediator during the reaction causing efficient electron transfer during the hydrolysis.

In order to study this hypothesis and understand the role of platinum during the hydrolysis in detail, X-ray absorption (including XANES and EXAFS) studies were performed on different samples. XAS studies will give valuable information about the structural information of two different catalysts of pure $LiCoO_2$ and 15 wt % Pt on $LiCoO_2$ during the hydrolysis of sodium borohydride for hydrogen generation. In particular,

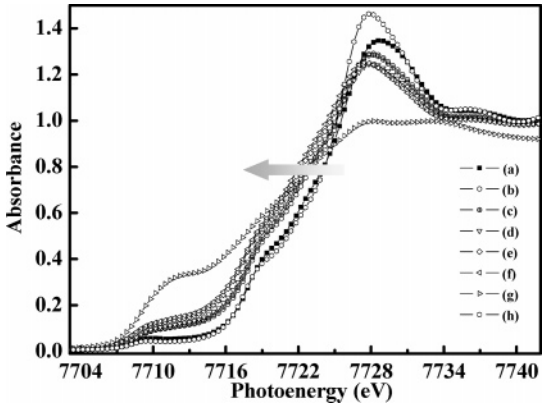

Figure 6. The *ex situ* Co K-edge XANES of 15% Pt−$LiCoO_2$ (a) before, (b) 1 h, (c) 2 h, (d) 3 h, (e) 4 h, and (f) 5 h of reaction, (g) Co foil, and (h) $LiCoO_2$.

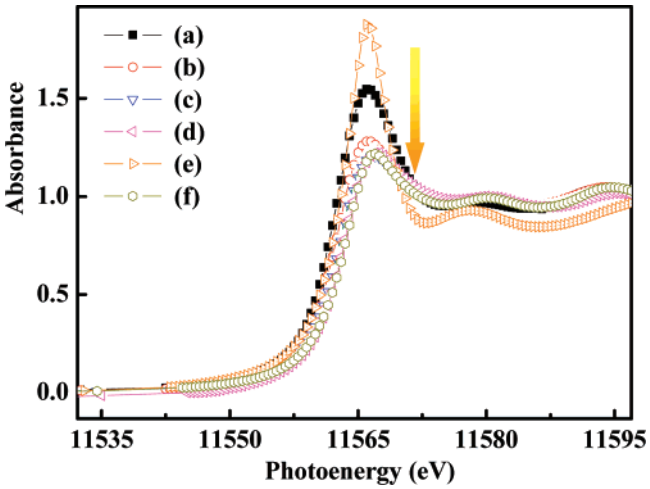

Figure 7. The *ex situ* Pt L_{III}-edge XANES of 15% Pt−$LiCoO_2$ (a) before, (b) 1 h, (c) 3 h, and (d) 5 h of reaction, (e) H_2PtCl_6, and (f) Pt foil.

EXAFS is a powerful tool yielding information about the local structure, coordination number, and distances from the absorbing metal without long-range order. These studies will also prove the electron-transfer mediation of Pt active centers which is crucial for effective catalytic action. Figure 6 shows the *ex situ* Co K-edge XANES for pure $LiCoO_2$ and 15 wt % Pt−$LiCoO_2$ before and after at 1, 2, 3, 4, and 5 h of reaction time. It was observed that there is no shift in the XANES pattern for pure $LiCoO_2$ for the reaction time of 5 h. The XANES spectra of 15 wt % Pt on $LiCoO_2$ changed significantly to lower energy values with time, indicating the formation of Co metal as the reaction proceeds. The shift in the near-edge region suggests that Pt nanoparticles played a major role, causing the reduction of Co^{3+} to Co metal with liberation of hydrogen. XANES of the Co K-edge gives valuable information about the role of platinum in the catalysis reaction.

Figure 7 shows the *ex situ* Pt L_{III}-edge for 15 wt % Pt−$LiCoO_2$ before and after at 1, 3, and 5 h of reaction time completion. It was observed that the white line intensity for 15 wt % Pt−$LiCoO_2$ before the reaction suggests the mixed oxidation state for platinum. After the reaction time of 5 h, the white line intensity is decreased as compared with 15 wt % Pt−$LiCoO_2$ (before reaction). It suggests that during this time period, Pt ions are converted to Pt atoms since heavy platinum atoms are preferred to form the more stable metal state. The finding is also supported by the X-ray photoelectron spectroscopic analysis which showed the higher ratio of Pt(0) to

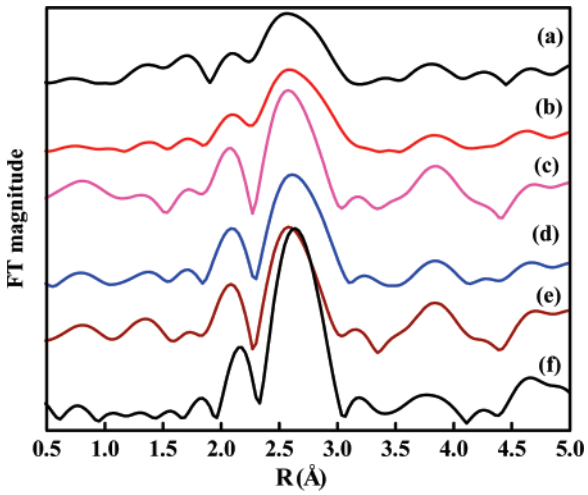

Figure 8. Fourier transforms of Pt L_{III}-edge $k^3\chi(k)$ EXAFS spectra (R space) of 15% Pt−$LiCoO_2$ (a) before, (b) 1 h, (c) 2 h, (d) 3 h, and (e) 4 h of reaction, and (f) Pt foil.

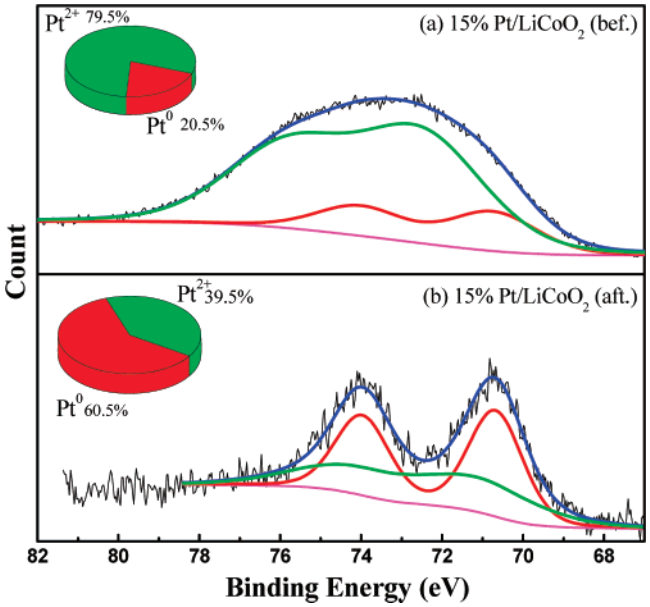

Figure 9. XPS measurements of 15% Pt−$LiCoO_2$ (a) before and (b) after reaction.

Pt(2+) content of 1.5 after reaction completion time as against the ratio of 0.26 before the start of the reaction. This study is used to investigate the changes in the surface structure of catalyst during the catalysis reaction. The bond length and coordination number are evaluated after fitting the data, which will give information about surface structure of catalyst. Figure 8 shows the Fourier transforms of Pt L_{III}-edge $k^3\chi(k)$ EXAFS spectrum (R space) for 15 wt % Pt−$LiCoO_2$ before and after 1, 3, and 5 h of reaction time. The broad peak observed in the region 2.5 Å to 2.7 Å of R space contribution indicates the presence of cobalt, whereas the R space intensity contribution at the value of 2.8 Å comes from the first shell of Pt−Pt coordination. It was observed that there is an increase in the intensity for the first shell of Pt−Pt during the course of reaction and a peak becomes narrow. It is well-known that for the higher oxidation state, its reduced ion is smaller and bonding length becomes smaller. Figure 9 shows the XPS measurements of 15% Pt−$LiCoO_2$ (a) before and (b) after reaction completion. It was observed from the XPS that before the catalysis reaction of Pt, it exists in a mixed oxidation state as reflected by the broad peak in the R space of EXAFS spectrum. During H_2 production

TABLE 2: Coordination Number (CN) and Radial Distances of 15 wt % Pt−$LiCoO_2$ for Different Time Periods

time	absorbing metal	scattering metal	CN	radial distance, r (Å)
before	Pt	Pt	8 ± 1.2	2.53 ± 0.32
1 h	Pt	Co	0.6 ± 0.2	2.46 ± 0.04
	Pt	Pt	9 ± 1.1	2.85 ± 0.56
2 h	Pt	Co	1.0 ± 0.2	2.55 ± 0.01
	Pt	Pt	11.2 ± 0.7	2.71 ± 0.62
3 h	Pt	Co	1.3 ± 0.2	2.62 ± 0.02
	Pt	Pt	10.8 ± 0.7	2.90 ± 0.34
4 h	Pt	Co	0.8 ± 0.3	2.56 ± 0.17
	Pt	Pt	10.9 ± 0.7	2.92 ± 0.31

with time, Pt ions are reduced to Pt metal (60.5%) over the time period step by step causing the peak in the R space of EXAFS spectrum to become sharp with time.

Table 2 shows the corresponding coordination number and radial distance of 15 wt % Pt−$LiCoO_2$ during the hydrolysis for 1, 2, 3, and 4 h of reaction time completion. It is very interesting to study the change in the coordination number and bond lengths during the course of the catalysis reaction. The coordination number for Pt−Pt is increased from an initial value of 8 to 11, indicating that more Pt is reduced as the reaction is progressed, and these reduced Pt atoms aggregate together resulting in the higher coordination number for Pt. Before the start of the reaction, the Pt environment is without Co since Co ions exist in $LiCoO_2$ support. Thus, the Pt−Co coordination number is very low in the beginning which increases as the reaction proceeds. It is assumed that Pt helps in the hydrogen generation, causing the reduction of Co ions to Co metal as reflected by the increase in the coordination number of Pt−Co. After 3 h of reaction time, the coordination number decreases, which is manifested as a result of Pt−Pt aggregation as discussed earlier.

We have generalized the results obtained from structural investigation using a synchrotron radiation source to get the insight into the mechanism of the overall catalysis process of hydrogen production using Pt−$LiCoO_2$. We propose a contribution from two separate processes that decides the catalytic activity of the composite catalyst in hydrogen production. The active nanocenters of Pt are surrounded by BH_4 ions because of a high molar ratio of $[BH_4]/[Pt]$ which causes easy removal of H ions from BH_4 ions as a result of electron transfer form BH_4 ions through the catalyst in the first process. On the other hand, H_2O absorbed on $LiCoO_2$ causes a weakening of H−OH, favoring the reduction of H^+-liberating H_2 from the solution in the second process. In this case, Pt or Co ions in the composite absorbed the electrons and results in the formation of metallic species by reduction of the metal ions. The evidence for this comes from XANES, EXAFS, and XPS measurements which showed the higher ratios of Pt and Co metal on the surface of composite during the hydrolysis. However, for the catalytic activity of pure $LiCoO_2$, there is no change in the valency of cobalt found which accounts for the absence of any electron-transfer resulting in the lowering of hydrogen production rate. The role of platinum is very crucial in the charge-transfer process, as there is no evidence of Co reduction using pure $LiCoO_2$ as a catalyst from XANES Co K-edge spectra analysis. The concentration, particle size distribution, and local environment of the active catalyst are also the keys in deciding the overall catalytic activity. We believe that Pt atoms play a role of mediator in electron-transfer causing the increased metal content, which may be beneficial for the regeneration of the catalyst surface. The higher density distribution of the Pt atom favors the second process as a result of increased charge

propagation due to increase in Pt concentration. However, more than 15 wt % density of platinum on $LiCoO_2$ result in the lowering of hydrogen generation rates because of the presence of Co_3O_4 impurity as confirmed by XRD, which will lower the catalytic efficiency of the composite catalyst. Thus, *ex situ* XANES and EXAFS investigations of the composite catalyst provided valuable information about the structural changes occurring during the hydrolysis reaction.

4. Conclusions

We have successfully synthesized Pt−$LiCoO_2$ composites using the impregnation method, and the catalytic activities were investigated by hydrogen generation rates. Characterization using XRD, TEM, and ICP-AES confirmed the Pt nanoparticle loading on $LiCoO_2$: 15 wt % Pt−$LiCoO_2$ was found to be an effective catalyst for hydrogen production as suggested by higher generation rates. XRD, XANES, and EXAFS using a synchrotron radiation source *ex situ* studies showed the changes in the local structure, valence, and coordination of absorbing Pt and Co atoms during the catalysis reaction. On the basis of XANES and EXAFS results, we proposed the mechanism for the hydrogen generation using Pt−$LiCoO_2$ catalyst that involves the discharge of the electron through the catalyst to the $LiCoO_2$ support, resulting in generation of hydrogen with simultaneous reduction of platinum and cobalt ions.

Acknowledgment. The authors would like thank the National Science Council of Taiwan for financially supporting this research under Contract No. NSC 95-2113-M-002-009.

References and Notes

(1) Suzuki, Y. *Int. J. Hydrogen Energy* **1982**, *7*, 227.
(2) Bockris, J. O. M. *Int. J. Hydrogen Energy* **1981**, *6*, 223.
(3) Asahi, R.; Morikawa, T.; Ohwaki, T.; Aoki, K.; Taga, Y. *Science* **2001**, *293*, 269.
(4) Scholz, F.; Schröder, U. *Nature Biotechnol.* **2003**, *21*, 9.
(5) Debabrata, D.; Veziro, T. N. *Int. J. Hydrogen Energy* **2001**, *26*, 13.
(6) Kong, V.; Foulkes, C. Y.; Kirk, F. R.; Hinatsu, D. W. *Int. J. Hydrogen Energy* **1999**, *24*, 665.
(7) Schlesinger, H. I.; Brown, H. C.; Finholt, A. E.; Gilbreath, J. R.; Hoekstra, H. R.; Hyde, E. K. *J. Am. Chem. Soc.* **1953**, *75*, 215.
(8) Amendola, S. C.; Ortega, J. V.; Wu, Y. (Millennium Cell, Inc., Eatontown, NJ). U.S. Patent 6,670,444, 2003.
(9) Amendola, S. C.; Sharp-Goldman, S. L.; Janjua, M. S.; Spencer, N. C.; Kelley, M. T.; Petillo, P. J.; Binder, M. *Int. J. Hydrogen Energy* **2000**, *25* 969.
(10) Kim, J.-H.; Lee, H.; Han, S.-C.; Kim, H.-S.; Song, M.-S.; Lee, J.-Y. *Int. J. Hydrogen Energy* **2004**, *29* 263−267.
(11) Amendola, S.; Onnerud, P.; Kelley, M. T.; Binder, M. *Talanta* **1999**, *49*, 267−277.
(12) Chuan, W.; Huaming, Z.; Baolian, Y. *Catal. Today* **2004**, *93*, 477.
(13) Brown, H. C.; Brown, C. A. *J. Am. Chem. Soc.* **1962**, *84*, 1493.
(14) Davis, R. E.; Bromels, E.; Kibby, C. L. *J. Am. Chem. Soc.* **1962**, *84*, 885.
(15) Shang, Y.; Chen, R. *Energy Fuels* **2006**, *20*, 2142.
(16) Davis, R. E.; Swain, C. G. *J. Am. Chem. Soc.* **1960**, *82*, 5949.
(17) Guella, G.; Zanchetta, C.; Patton, B.; Miotello, A. *J. Phys. Chem. B* **2006**, *110*, 17024.
(18) van Dam, H. E.; van Bekkum, H. *J. Catal.* **1991**, *131*, 335.
(19) Russell, A. E.; Rose, A. *Chem. Rev.* **2004**, *104*, 4613.
(20) De Miguel, S. R.; Scelza, O. A.; Román-Martínez, M. C.; Salinas-Martínez de Lecea, C.; Cazorla-Amorós, D.; Linares-Solano, A. *Appl. Catal. A* **1998**, *170*, 93.
(21) Adora, S.; Soldo-Olivier, Y.; Faure, R.; Durand, R.; Dartyge, E.; Baudelet, F. *J. Phys. Chem. B* **2001**, *105*, 10489.
(22) Kojima, Y.; Suzuki, K.-I.; Fukumoto, K.; Kawai, Y.; Kimbara, M.; Nakanishi, H. M. *J. Power Sources* **2004**, *125*, 22.
(23) Iwasawa, Y. *X-ray Absorption Fine Structure for Catalysts and Surfaces*; World Scientific: Singapore, 1996.
(24) Baba, Y.; Okada, S.; Yamaki, J.-I. *Solid State Ionics* **2002**, *148*, 311.
(25) Amendola, S. C.; Onnerud, P.; Kelly, M. T.; Petillo, P. J.; Sharp Goldman, S. L.; Binder, M. *J. Power Sources* **2000**, *85*, 186.